Development of a New High Dynamic Range Technique for Solar Flux Analysis Using Double-CCD Optical Camera

Mohamed Adel*‡, Adrian Peña-Lapuente**, Mohamed Rady***, Alaa Hamdy****

*Mechanical Engineering Department, Helwan University, 11792 Helwan, Cairo, Egypt

**Solar Thermal Department, National Renewable Energy Centre of Spain (CENER), 31621 Sarriguren, Navarra, Spain

***Mechanical Engineering Department, Faculty of Engineering, Rabigh, King Abdulaziz University, KSA

****Electronics, Communications and Computer Engineering Department, Helwan University, 11792 Helwan, Cairo, Egypt

(m.adel_helwan@yahoo.com, apena@cener.com, makrady@yahoo.com, alaa.hamdy@gmail.com)

‡Corresponding Author; Mohamed Adel, 1 Sherif Street, 11792 Helwan, Cairo, Egypt, Tel: +20 109 077 6722, m.adel_helwan@yahoo.com

Abstract- In solar central receiver (SCR) systems, camera-based tracking and control strategies have been widely developed and tested. The camera, usually with a single CCD, captures images of the sun reflected by thousands of heliostats on the central receiver. The captured images are then analysed to allow the evaluation of solar flux. For accurate analysis process, the camera must have a high dynamic range (HDR) to give real and accurate information about the captured scene. In the present article, a new methodology has been developed using a double-CCD optical camera for improvement of dynamic range of the captured solar flux image. An experimental calibration set-up is adopted for accurate estimation of the camera response function. The double-CCD camera is used for acquiring two images at the same instant with two different levels of exposure. The two captured images are then merged into a single HDR image using a new proposed weighting function. The enhanced optical performance of the proposed weighting function has been demonstrated by comparison with the previous HDR image generation weighting functions at different levels of illumination. Investigation of the capability of the proposed methodology for the analysis of beam accuracy and optical quality of SCR systems show that the present proposed method leads to more accurate solar flux analysis because of the improvement in the resolution of details of the final merged image.

Keywords- High Dynamic Range Image; Weighting Function; Optical Quality; Beam Accuracy.

Nomenclature

CCD	Charge-Coupled Device
CRF	Camera Response Function
CSP	Concentrating Solar Power
HDR	High Dynamic Range
I	Exposure value (W. sec)
LDR	Low Dynamic Range
M	Number of pixels of image
SCR	Solar Central Receivers
SNR	Signal-to-Noise Ratio
t	Exposure time (sec)
w	Weight of pixel (0:1)
x	Irradiance (watt)
y	Observation of pixel
z	Input pixel value
β	Roll-off factor

1. Introduction

The evaluation of concentrating solar power (CSP) systems optical performance is an important task during development and operation phases of solar power plants. In the development phase, it helps to improve the reflecting and receiving systems design. During the operation phase, it represents a major factor affecting the efficiency of the plant and performance losses induced by undesirable errors in the tracking system. The optical performance of a CSP system is

basically measured by the beam accuracy and the optical quality. The beam accuracy is a measure of the ability of mirrors to accurately reflect the sunlight on the receiver. The optical quality characterizes the shape of the reflected light with respect to the ideal shape. In order to evaluate the optical performance of solar central receiver (SCR) systems, the flux distribution of the reflected light has to be estimated.

The state-of-the-art method for heliostat characterization and calibration is to measure the flux reflected on a calibration target [1]. The tracking accuracy is frequently determined by the measured position of the reflected beam centre on a target [2]. Measurement and estimation methods of incident solar flux on central receivers of SCR systems are classified into direct and indirect methods [3]. In [4], a method for estimation of solar radiation on surfaces at different orientations has been presented. For evaluation of global solar radiation data, different methods have been presented in [5-7]. In [8], an experimental study for evaluation of solar flux distribution on a flat receiver has been presented. The method presented in [8] has been carried out following different conditions than conditions of methods presented in [9-11]. Indirect measurement principles are being used since the end of the 1970s [12]. Almost all indirect methods use single CCD digital cameras to characterize flux distributions. Cameras are used to image the flux distribution of the reflected light which is then analysed.

Since the capturing process is affected by different noise sources, the dynamic range of the capturing camera must be high enough to reliably estimate the captured flux. In weak flux intensity areas, the signal-to-noise ratio (SNR) of the captured image is low. Small values of exposure time results in a loss of information in low intensity areas. This calls for long exposure time of the camera to increase its sensitivity to differences at small values of flux intensities. However, in areas of high intensity, shorter exposure time is required to avoid image saturation.

Since the first work presented in [13], the standard way to build high dynamic range (HDR) images has been based on combining some images captured with different exposure times. The first step in the process of creating a HDR image is the alignment of the original images [14]. This step is subjected to alignment errors due to the quick and continuous movement of the sun light spot on the target.

The algorithms proposed in the literature differ in the strategy used to combine the low dynamic range (LDR) images. In [13,15], using certainty functions, the authors weight the observations taken with various exposures to provide the final image. In [16-19], a linear camera response function (CRF) has been assumed and the final output pixel has been picked based on the observation with the longest unsaturated exposure time to reduce the quantization noise. In [20], a cut-and-paste method to increase the dynamic range has been suggested. In [21], an arbitrary camera response has been assumed which is determined as a part of the algorithm. In [22], the authors perform a weighted average to increase the dynamic range of images.

The present work aims to avoid the alignment step and estimate the flux distribution on a target using a camera with two CCD sensors. Both sensors receive almost the same incident light by means of a prism that divides incoming light into both sensors [23]. Each sensor is configured individually to allow different exposure times. The obtained images are then merged into one with a higher dynamic range. In terms of solar flux analysis, this would allow to accurately retrieve the border low energy areas, increase the magnitude of resolution, and analyse the high energy areas.

The major contribution of the present work can be summarised as follows:

- Employment of double-CCD camera for obtaining HDR images for the analysis of solar flux in SCR systems using images captured at the same time.
- Accurate estimation of camera response function (CRF) by adopting an experimental calibration process which can be applied for any capturing system.
- Development of a new weighting function for obtaining the merged image which shows superior performance as compared to existing weighting functions reported in the literature.
- Demonstration of the capability of the new developed technique for accurate optical analysis of reflected solar flux in SCR systems.

The present article is organised following the procedure adopted in developing the proposed technique as follows. The experimental set-up used to estimate the response function of each sensor of the double CCD camera is described in Section 2. The calibrated double-CCD camera is used for acquiring two images at the same instant with two different levels of exposure. The two captured images are then merged into a single HDR image using a new proposed weighting function. Section 3 discusses the method used to obtain the final HDR image and presents our new proposed weighting function. The enhanced optical performance of the proposed weighting function has been demonstrated by comparison with the previous HDR image generation weighting functions at different levels of illumination. Investigation of the capability of the proposed methodology for the analysis of beam accuracy and optical quality of SCR systems are reported in Section 4.

2. Camera Response Function Estimation

The camera response function is an important requirement when performing the construction of HDR images. The CRF simply relates quantized image pixel values with physical incoming light [24]. The CRF can be obtained through calibration procedures, or estimated from a set of LDR images with different exposure times. In our case, the camera is going to be calibrated to reach a more exact approach.

2.1. Calibration Procedure

A prism-based double-CCD camera (JAI AD-081 GE CCD) is used to capture two simultaneous images for the same scene at different exposure times. The camera captures

30 fps simultaneously via two video channels with a resolution of 1024 x 768 pixels. Based on the manufacturer data, the camera sensitivity is 0.34 Lux (On sensor, maximum gain, shutter off, and 50% video). When JAI SDK control tool is executed, AD-081GE is recognized as two imagers that can be handled as independent cameras [25]. An integrating sphere illuminated by a variable light source is used as a uniform light source. An irradiance sensor, which has an uncertainty of $\pm$ 2.5% of measurement, is used to measure the irradiance at the output port of the integrating sphere.

Fig. 1 shows the set-up of the calibration process. This process took place in a dark room to ensure uniform lighting conditions, so the calibrating sphere is the only irradiance source. Several images of the output port of the integrating sphere are captured by the camera at different irradiance values. The aperture and exposure times are kept constant. For each sensor, the averaged values of certain pixels of each captured image are plotted versus the exposure values. The

exposure value is the product of exposure time (in seconds) and irradiance value (in milliwatt). Fitting the values result in the response function of the sensor. For accurate fitting, the saturated pixels are ignored (255 counts for 8-bit data). Fig. 2 shows the estimated response function of each sensor. The uncertainty values of the response function are $\pm$ 2.6% and $\pm$ 3.2% for the first and second CCD, respectively.

3. HDR Range Image Reconstruction

Robertson et al. [22] present an algorithm based on a probabilistic formulation for increasing the dynamic range of digital images for known CRF. With a known response function, HDR images can be easily constructed by a weighted average of the input images. However, the weighting function used assigns non-zero weighting values to the saturated pixels in the LDR images, while these saturated pixels do not provide any information for the reconstruction process.
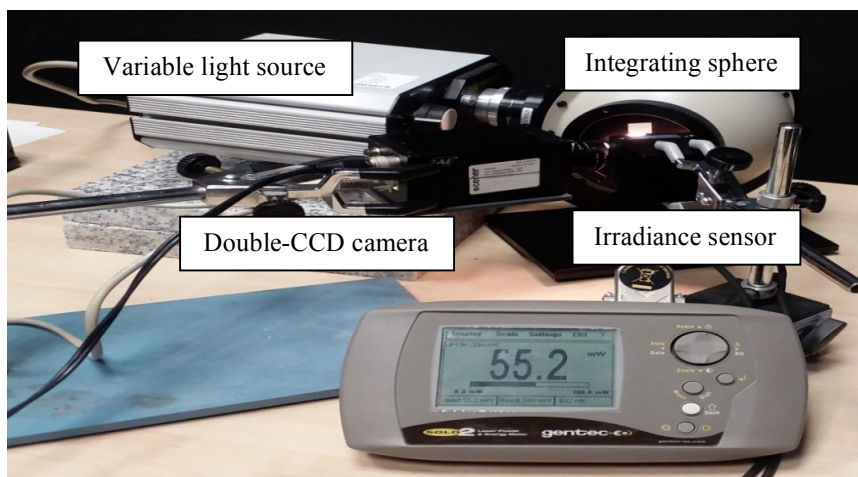
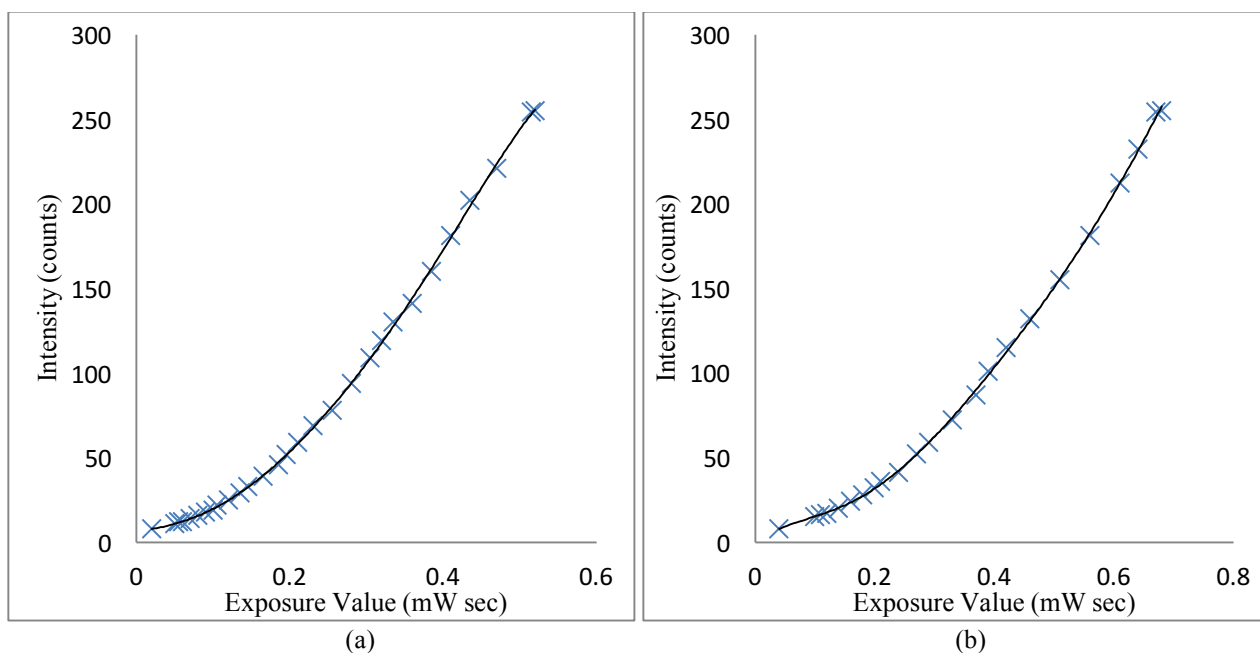

Fig. 1. Set-up of camera calibration process.

Fig. 2. Estimated response function of each sensor of the camera: (a) First sensor (exposure time of 5 milliseconds), (b) Second sensor (exposure time of 10 milliseconds).

3.1. HDR Image with Known Camera Response

According to our case, using the model of observation of Robertson et al. [22], there are two captured images (by sensor 1 and sensor 2) for the same scene with known exposure times (t_1 and t_2). Each image consists of M pixels. The jth pixel of the image is denoted as y_{1j} and y_{2j}. Therefore, $\{y_{1j}\}$ and $\{y_{2j}\}$ represent the known observations. The goal is to determine the underlying light values or irradiances, denoted by x_j, which give rise to the observations y_{1j} and y_{2j}. For HDR creation, Robertson et al. [22] proposed to weight pixels such that pixels coming from longer exposures have higher weights than pixels coming from shorter ones. The HDR assembly defined, when taking only two images, is obtained using:

$$x_j = \frac{w_{1j}\, t_1\, I_{1j} + w_{2j}\, t_2\, I_{2j}}{w_{1j}\, t_1{}^2 + w_{2j}\, t_2{}^2} \qquad (1)$$

Where w is the weight of the pixel obtained from the weighting function used, and I is the exposure value of the pixel. I_1 is obtained from the response function of the first sensor and I_2 from the response function of the second sensor.

The following section reviews the weighting functions used in the reconstruction of HDR images, discusses the effect of the weighting functions on the final merged image, and shows our proposed weighting function for HDR image generation.

3.2. Analysis of Existing Weighting Functions

In the construction of HDR images, the weighting functions are used to give some pixels more weight or influence on the final output pixels of the merged HDR image than other pixels. As the weighting values detect how the output pixel will be observed, the correct choice of the weighting function leads to the correct operation of the HDR construction algorithm. Some of the weighting functions that have been proposed in the literature are shown in Fig. 3 and Table 1 for 8-bit data images. The weighting functions convert pixel values of LDR images (from 0 to 255) to weights (from 0 to 1). These weights are used to obtain the final pixel value of HDR image.
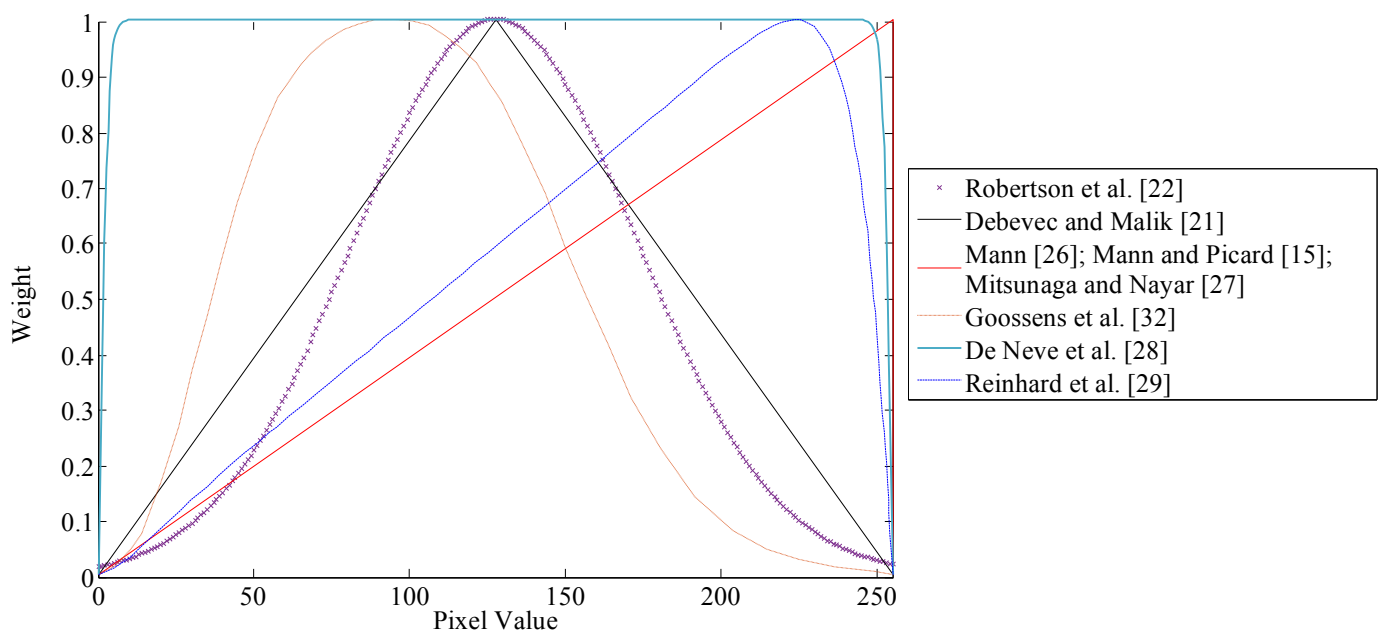

Fig. 3. Weighting functions used for HDR reconstruction.

Table 1. Previous weighting functions used for HDR image construction

Robertson et al. [22]	$w(z)=\exp\left(-\,4\cdot(z-127.5)^2/(127.5)^2\right)$
Debevec and Malik [21]	$w(z)=\begin{cases} z/127.5, & z \le 127.5 \\ (255-z)/127.5, & z > 127.5 \end{cases}$
Mann [26]; Mann and Picard [15]; Mitsunaga and Nayar [27]	$w(z)=\begin{cases} z/255, & z < 255 \\ 0, & z = 255 \end{cases}$
De Neve et al. [28]	$w(z)=\exp(-(z-127.5)/b(127.5)^a)$ Here, a and b are constants which were determined experimentally.
Reinhard et al. [29]	$w(z)=\begin{cases} (z/255)\left[1-((z/127.5)-1)^{12}\right], & z < 255 \\ 0, & z = 255 \end{cases}$

In [16-19], the authors weight the output pixels by only the one with the brightest (non-saturated) value. In [15,26], the authors select a weight related to the slope of the CRF. In [27], the authors weight the observations of the LDR images by the SNR. In [28], an exponential power function has been proposed to emphasize the middle of the exposure range. In [29-31], other weighting functions have been proposed where the maximum weighting value is shifted towards the high intensity pixels.

In [21], a triangular function has been proposed to give higher weight to exposures in which the value of the pixel is closer to the middle of the response function. In [22], the authors use a Gaussian function as a weighting function. In [32], the authors present HDR image reconstruction weighting scheme based on a camera noise model that incorporates different noise sources. This weighting function increases the SNR of the HDR image. But detailed knowledge of the capturing system would be required, and it is different for each capturing device.

In order to show the effect of different weighting functions on the final HDR image, a scene with abrupt changes in illumination has been chosen for performing this analysis. This choice represents a step function test for the weighting functions. For this purpose, a high quality poster for the image of Sun reflected on the sea was captured by the double-CCD camera to produce two grayscale images of the same scene with different exposure times as shown in Fig. 4. Then, Robertson et al.'s method for known response cameras is used to perform the merging process. The algorithm uses the estimated CRF and the weighting functions of Fig. 3 for weighting the pixels of the LDR images.

The weighting functions used in [15,26,27,29] weight the high intensity pixels with values higher than other pixels (near 1) and suddenly the weight drops to 0 for saturated pixels. This sudden change in weighting values causes sharp edges in the merged image between saturated pixels and neighbouring ones. This results in distorting the image as can be noted from the Sun reflection on the sea in Fig. 5a and Fig. 5b. In addition to this problem, the weighting function used in [28] weights almost all the pixels with the same value, so the HDR pixel value is considered as an averaged value of the input pixels. This results in missing details in the centre of the Sun in Fig. 5c.

The Gaussian weighting function used by Robertson et al. [22] and the triangle function used by Debevec and Malik [21] solve the problems discussed in the other functions. They weight pixels according to each pixel value. Pixels near the mean of the input pixel range (128 for 8-bit data) are weighted higher than pixels near the extremes of the input pixel range (0 and 255 for 8-bit data).

(a)   (b)

Fig. 4. Two image of the same scene captured at different exposure times: (a) 10 milliseconds and (b) 20 milliseconds.

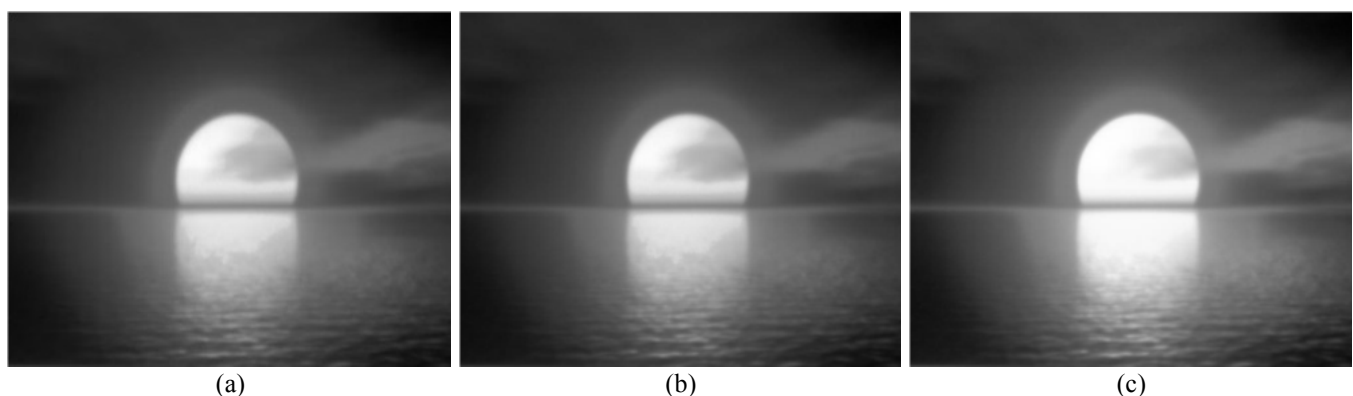(a)   (b)   (c)

Fig. 5. Merged images for the two images of Fig. 4 using the weighting functions proposed by: (a) Mitsunaga and Nayar [27], (b) Reinhard et al. [29] and (c) De Neve et al. [28].

3.3. Proposed Weighting Function

In the present work, in order to solve the inherent problems of the previous weighting functions, the implementation of a raised-cosine function as a weighting function for HDR image creation is proposed. The proposed function gives a higher weight to input data that are nearer to

$$w(z) = \begin{cases} 1, \\ \frac{1}{2}\left[1 + \cos\left(\frac{\pi}{127.5\,\beta}\left[|z - 127.5| - \frac{127.5\,(1-\beta)}{2}\right]\right)\right], \\ 0, \end{cases}$$

Where β is the roll-off factor that controls the form of the function and provides the function with a degree of adaptability.

As the extreme values of the input range (0 and 255) do not contain valuable information, a roll-off factor of 1 can be applied in Eq. (2) to ignore them. The weighting function can be expressed as:

$$w(z) = \begin{cases} \frac{1}{2}\left(1 + \cos\left(\frac{\pi\,.\,(z+127.5)}{127.5}\right)\right), & z \in [0,255] \\ 0, & otherwise \end{cases} \quad (3)$$

One of the most common noise sources, at low pixel values, is the average dark signal. It is a constant value (offset value) that is added to the actual signal value and can be different for different cameras. It is typically illustrated in data sheets of cameras, and also can be measured experimentally. It is generated due to dark current, which refers to unwanted free electrons generated due to thermal energy. Dark signal measurement needs to be done in fully dark conditions to shield sensors of the camera from incoming light. For the camera used in the present work, the dark current generates an offset of around 8 counts, which is added to each actual pixel value. When pixels have a value of 8 counts or less, those pixels have useless information, so they should be ignored. To do this, our function can be modified using a different roll-off factor, taking advantage of its adaptability.

Applying a roll-off factor between 0 and 1 in Eq. (2) results in giving a weight of zero not only to the two extremes values of the input range, but also to some values near these extremes. The number of ignored pixels depends on the value of the roll-off factor used. As we want to ignore only the lowest values affected by dark current noise, a combined weighting function with two roll-off factors is proposed, as shown in Fig. 6. For high intensity pixel values, only the saturated pixels (255) will be ignored. This can be achieved using Eq. (3). On the other hand, for low pixel values, the lowest values (0 to offset value) will be ignored. In this case, the roll-off factor can be calculated according to the offset value a using:

$$\beta = 1 - \frac{2}{127.5}\,a \quad (4)$$

the mean of the input pixel range as compared to Gaussian and triangle weighting functions and ignores saturated pixels. If saturation is found in one of the LDR images, the final image will take the information of that pixel only from the non-saturated one. If the input pixel value is denoted as z and the corresponding weight as w, the raised-cosine weighting function for 8 bit data can be defined as:

$$\begin{array}{ll} |z - 127.5| \leq \frac{127.5\,(1-\beta)}{2} \\[2mm] \frac{127.5\,(1-\beta)}{2} < |z - 127.5| \leq \frac{127.5\,(1+\beta)}{2} \qquad (2) \\[2mm] otherwise \end{array}$$

3.4. Analysis of Proposed Weighting Function

The present section is devoted to show the enhanced performance of the proposed weighting method at different levels of illumination. A scene with heterogeneous high and low illumination areas has been chosen for performing this analysis. This choice tests the capability of the proposed weighing function to correctly capture these heterogeneous details of the scene. For this purpose, a high quality poster exhibiting these features was captured by the double-CCD camera to produce two grayscale images of the same scene with different exposure times (10 milliseconds and 20 milliseconds) as shown in Fig. 7. The images of Fig. 8 are the merged images of the two LDR captured images obtained using different weighting functions. For analysing results and owing to the fact that the eye cannot distinguish pixels placed together of similar colours, the pixel values along the same line passing through low and high illuminations in the middle of all images of Fig. 7 and Fig. 8 are represented in Fig. 9. The represented line is marked in the image of Fig 7a.
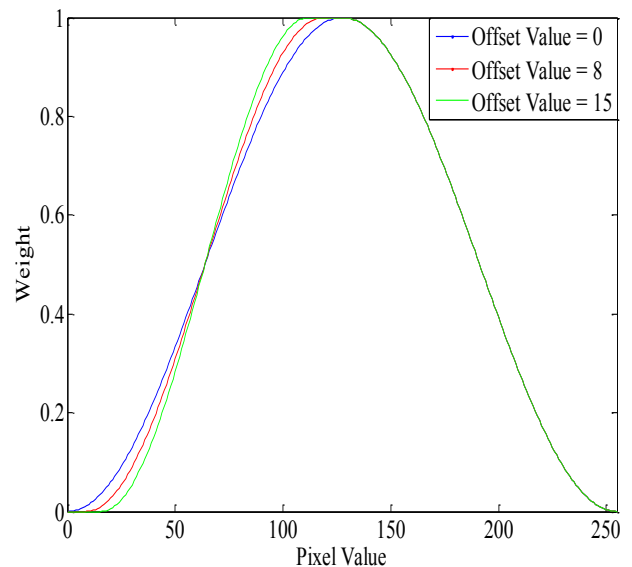

Fig. 6. Proposed weighting function according to the constant offset value obtained from the dark current level.
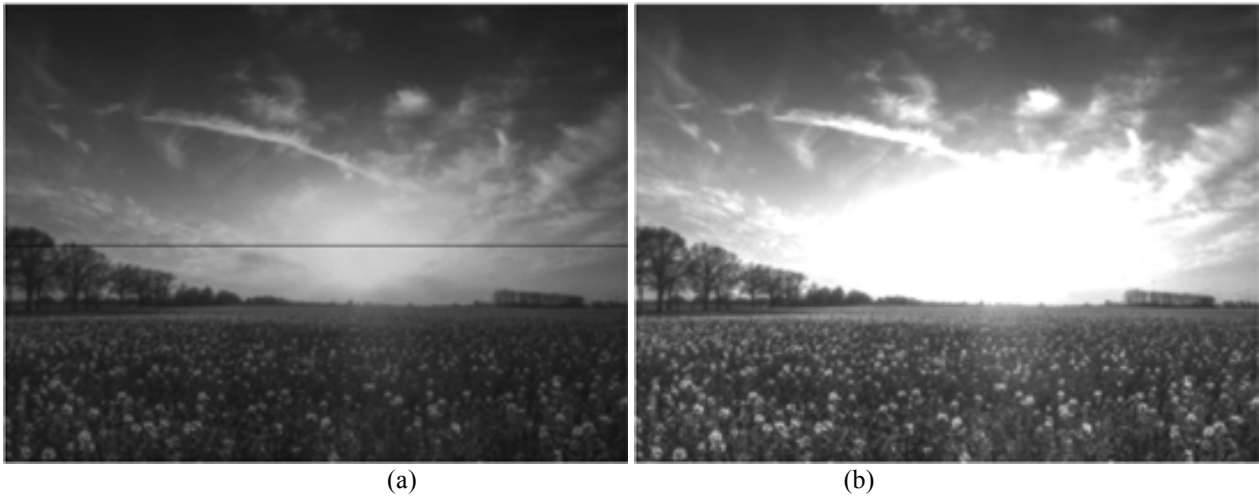
(a) (b)

Fig. 7. Two images with different exposure times captured with the double-CCD camera: (a) 10 milliseconds (the marked line indicates the position of pixels represented in Fig. 9) and (b) 20 milliseconds.

(a) (b)

(c) (d)

Fig. 8. Merged images for the two images of Fig. 7 using: the weighting functions proposed by (a) Robertson et al. [22], (b) De Neve et al. [28] and (c) Reinhard et al. [29], and (d) present proposed weighting function.
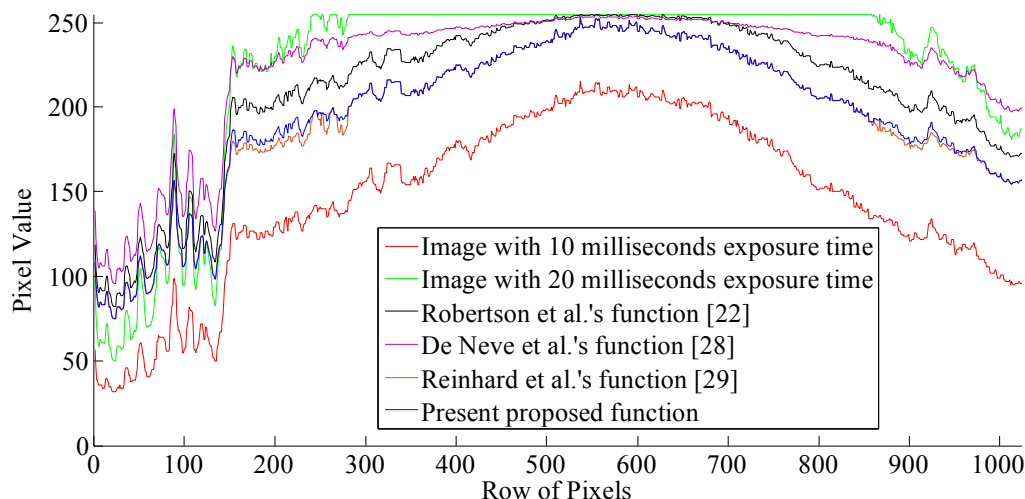
Fig. 9. Comparison of pixel values along the line shown in Fig. 7a of merged images using different weighting functions.

In image analysis applications, the behaviour of each HDR observed pixel has to follow the behaviour of the LDR pixels. Fig. 9 shows that there are some pixels that seem to be saturated in the final merged image using Robertson et al.'s and De Neve et al.'s weighting functions. This saturation results in missing some details in the final merged image as can be noted in images of Fig. 8a and Fig. 8b. For Robertson et al.'s image, the missing details introduced from not ignoring the saturated pixels in the original images during the weighting process. For De Neve et al.'s image, although the saturated pixels are ignored, the weighting function gives almost all other pixels high weights. This increases the observed pixels values, and changes their behaviour. On the other hand, Reinhard et al.'s function solves the problem occurring at saturation and the pixels behaviour seems to be the same as the pixels behaviour obtained by the present proposed function. However, as discussed before, it causes sharp edges between the saturated pixels and the neighbouring ones. These sharp edges decrease the resolution of the merged image in these areas as can be noted in the image of Fig. 8c and in the sudden changes that appeared around the pixel value of 180 in Fig. 9. Although over-saturation is found in one of the input images (see image of Fig. 7b), using the proposed weighting function solves the problems encountered using the other weighting functions. So this finally results in a high resolution output image (Fig. 8d). The image behaviour simulates the original scene giving real information as noted in Fig. 9.

4. Optical Analysis

The aim of this section is to demonstrate the capability of the present proposed methodology for optical analysis of SCR systems. The optical performance of SCR systems can be evaluated by analyzing both the beam accuracy and the optical quality of the reflected light. The concentrated flux distribution at the receiver is controlled by the aiming strategy of thousands of heliostats in the field to accomplish the specific requirements of solar-thermal conversion processes. The optical quality is crucial for accurate determination of the total energy sum and its distribution and concentration on the receiving plane. The beam accuracy, also referred to as centering, is measured by the deviation of the centroid of a certain heliostat flux map from the well-known geometrical centre of the target. Calibration and control of heliostat tracking system seek to minimize centering error and increase the beam accuracy.

The heat flux map at the target receiver can be constructed using the information embedded in the HDR image. The value of each pixel of the HDR image represents an indirect measure of heat flux intensity. A constant conversion factor to convert pixel values into heat flux units was assumed by Marwan Mokhtar et al. [33]. However, accurate conversion can be performed using the camera response function depicted in Fig. 2. Further details on available conversion techniques are presented by Marc Röger et al. [34]. In the present study, experiments have been carried out by simulating the solar flux coming from a heliostat field using a lamp directed to form a spot on a flat plate, as a first approximation to the real case.

4.1. Optical Quality

Using the calibrated double-CCD camera, two grayscale images were captured at different exposure times (10 milliseconds and 20 milliseconds) as shown in Fig. 10a and Fig. 10b. Fig. 10c shows the HDR merged image for the two LDR captured images. The HDR image was represented by Robertson et al.'s method for known CRF using the estimated CRF and applying the proposed weighting function.

In order to increase the visibility of the details, the grayscale images of Fig. 10 are displayed in false colours in Fig. 11. Images of Fig. 11 show that applying the proposed method solves the problem of pixels saturation in the higher exposed image as can be noted in the middle of the spots of Fig. 10 images. Moreover, the details absent in separate LDR images can be found in the HDR merged image. This can be noted in the area marked with black circles in images of Fig. 11. In the right part of the circle, one can note that there are some details that are lost in the lower exposed image, while

they can be seen in the higher exposed image. On the contrary, in the left part of the circle, the lost details are in the higher exposed image.

For the LDR images and the HDR one, high and low illumination pixels have been plotted. Fig. 12 represents the same row of pixels in all images of Fig. 10 passing through the middle of the spot. The HDR image pixel values differ from both LDR images pixel values. However, the behaviour is very similar to at least one of them. In case of low pixel values, it follows the higher exposed image behaviour where

the low light areas are well represented. In case of high pixel values, it follows the lower exposed one where the high light areas are well represented. Also, the behaviour in case of saturation is the same as the lower exposed image behaviour. This means that saturated pixels that contain no information about the captured scene are ignored, leading, in this way, to a clear enhancement in the resolution of the final HDR image, which should lead to a better characterization of the optical quality of the heliostat. This last fact will be subject of a deeper study, and some field test will be performed in the future.
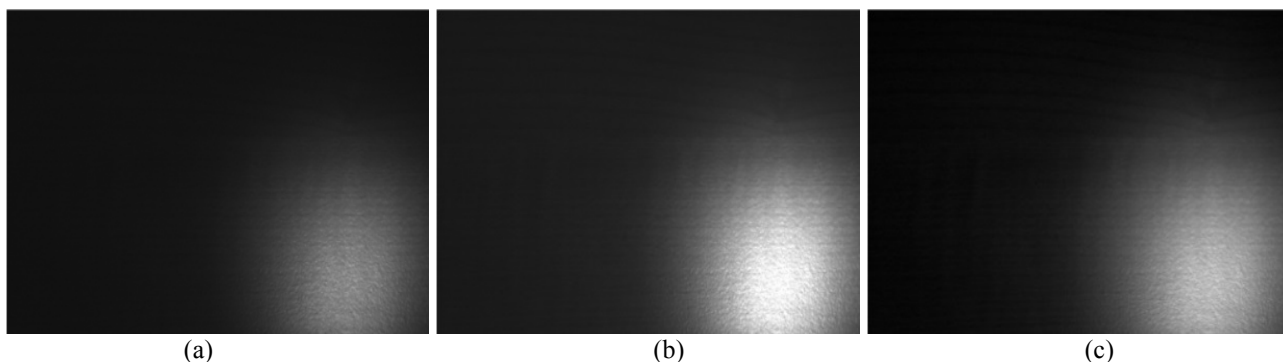

(a)　　　　　　　　　　　　(b)　　　　　　　　　　　　(c)

Fig. 10. Two images with different exposure times captured by the double-CCD camera: (a) 10 milliseconds and (b) 20 milliseconds, and (c) the merged HDR image with the present proposed method.
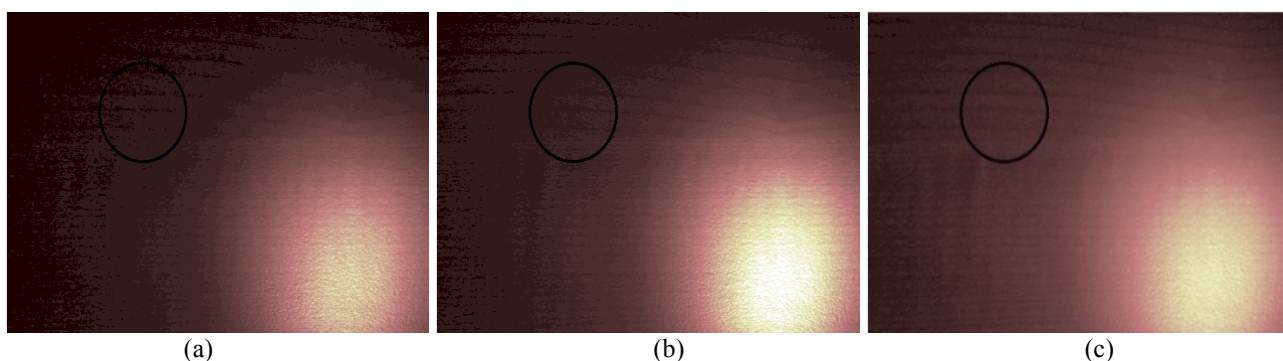

(a)　　　　　　　　　　　　(b)　　　　　　　　　　　　(c)

Fig. 11. False colour images for images of Fig. 10: (a) 10 milliseconds image, (b) 20 milliseconds image and (c) the merged HDR image with the present proposed method.
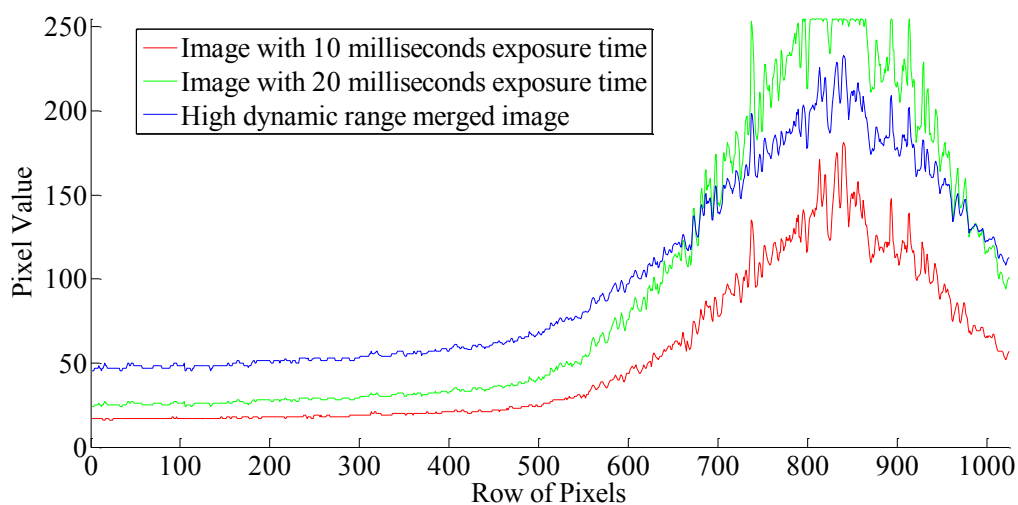

Fig. 12. Comparison of pixel values on a horizontal line between the two base LDR images and the merged HDR image.

4.2. Beam Accuracy

In order to draw meaningful conclusions and compare the performance of different weighting functions for the analysis of beam accuracy, 20 pairs of images were captured for the same scene by both sensors of the double-CCD camera in a similar way to the previous test. Every couple of images was merged to one image applying different weighting functions. The merged images were then masked and different thresholds were applied. Threshold value selection differs from one case to another because it depends on the pixel values of the segmented image. A mask was applied for all images to discard parts of the image that are not of our interest. A threshold was then chosen where the pixels that are greater than that threshold were only considered as part of the solar spot. For all merged images, the centre of mass (centroid) of the segmented spot was calculated. The chosen threshold values were between 0.45 and 0.90. Values lower than 0.45 were discarded for reasons of segmentation of the spot. Small thresholds incorrectly segment parts of the image as part of the spot. The real centroid of each image was calculated for each weighting function and assumed to be the averaged centroid of all images.

To compare different weighting functions, the root mean square (RMS) value of the distances between the calculated centroid of each image and the averaged value is used as a figure of merit. The obtained results are represented in Fig. 13. It can be noted that the RMS value for almost all thresholds is lower in case of applying the present proposed method. The centroids for the case in which the images have been merged using the present proposed weighting function exhibit less deviation from the averaged value than the other cases. As mentioned before, the beam accuracy of SCR systems is measured by the determination of the centroid of the solar flux reflected on the target and its deviation from the aiming point. So according to the obtained results, the centroid of the solar flux reflected on the target can be better estimated from the merged HDR image constructed by the present proposed method.

5. Conclusion

Image-based solar flux analysis systems require a HDR image that contains all details of low and high illumination areas of the captured solar flux. The present study proposes a new methodology using a double CCD camera for improvement of dynamic range of captured solar images. To avoid the misalignment error between images, the double-CCD camera is used to capture two images at the same instant with different levels of exposure. Merging both images results in obtaining a new image with a higher dynamic range. An experimental calibration process is recommended and applied for accurate estimation of the CRF. The process is considered as an initial calibration step, which can be applied for any capturing system. It needs to be performed only once, but it could be performed periodically so as to recalibrate the camera after aging. As the pixel values of the merged image are weighted, a new modified raised cosine weighting function is proposed, in order to reduce some distortions that appear when using other weighting functions, and therefore creating an accurate HDR image for solar flux analysis. Comparisons between HDR images obtained by applying the new proposed weighting function and previous HDR image fusion weighting functions show dynamic range improvement of the optical camera in terms of the details and the behaviour of the final HDR image.

The capability of the present methodology for accurate analysis of optical quality and beam accuracy of SCR systems has been demonstrated by performing indoor tests. Future work should focus on studying the performance and quantifying different sources of errors of the developed technique under real conditions by performing a series of outdoor experiments. Ray tracing simulations can help in this regard to provide reference images of flux density distributions.
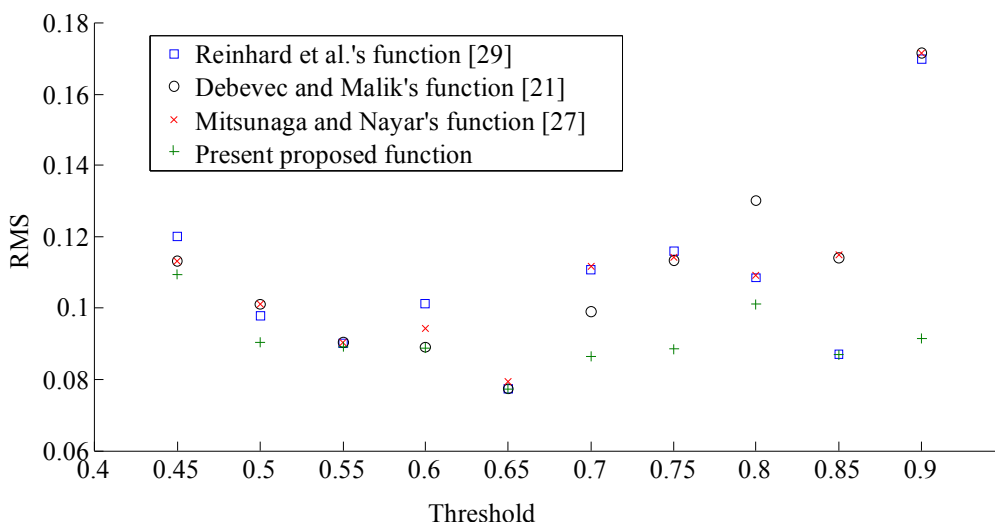

Fig. 13. Representation of RMS values of spot centroid calculations of the merged images applying different weighting functions and different threshold values.

References

[1] A. Pfahl, J. Coventry, M. Röger, F. Wolfertstetter, J. F. Vásquez-Arango, F. Gross, M. Arjomandi, P. Schwarzbözl, M. Geiger, and P. Liedke, "Progress in heliostat development" , *Solar Energy*, vol. 152, pp. 3-37, August 2017.

[2] M. Berenguel, F. R. Rubio, A. Valverde, P. J. Lara, M. R. Arahal, E. F. Camacho, and M. López, "An artificial vision-based control system for automatic heliostat positioning offset correction in a central receiver solar power plant" , *Solar Energy*, vol. 76, no. 5, pp. 563-575, January 2004.

[3] M. Röger, P. Herrmann, S. Ulmer, M. Ebert, C. Prahl, and F. Göhring, "Techniques to Measure Solar Flux Density Distribution on Large-Scale Receivers", *Journal of Solar Energy Engineering*, vol. 136, no. 3, p. 031013, May 2014.

[4] A. Ibrahim, A. A. El-Sebaii, M. R. I. Ramadan, and S. M. ElBroullesy, "Estimation of solar irradiance on inclined surfaces facing south in Tanta, Egypt", *International Journal of Renewable Energy Research*, vol. 1, no. 1, pp. 18-25, March 2011.

[5] M. Demirtas, M. Yesilbudak, S. Sagiroglu and I. Colak, "Prediction of solar radiation using meteorological data", *International Conference on Renewable Energy Research and Applications, ICRERA*, Nagasaki, Japan, pp. 1-4, 11-14 November 2012.

[6] M. Jazayeri, S. Uysal, and K. Jazayeri, "A case study on solar data collection and effects of the Sun's position in the sky on solar panel output characterization in Northern Cyprus", *International Conference on Renewable Energy Research and Applications, ICRERA*, Madrid, Spain, pp. 184-189, 20-23 October 2013.

[7] R. Al-Hajj, A. Assi, and F. Batch, "An evolutionary computing approach for estimating global solar radiation", *International Conference on Renewable Energy Research and Applications, ICRERA*, Birmingham, UK, pp. 285-290, 20-23 November 2016.

[8] P. M. Gadhe, S. N. Sapali, and G. N. Kulkarni, "Experimental evaluation of the solar flux distribution on the flat receiver of a model heliostat system", *International Journal of Renewable Energy Research*, vol. 8, no. 2, pp. 878-887, June 2018.

[9] A. Al-Ghasem, G. Tashtoush, and M. Aladeemy, "Experimental study of tracking 2-D compound parabolic concentrator(CPC) with flat plate absorber", *International Conference on Renewable Energy Research and Applications, ICRERA,* Madrid, Spain, pp. 779-782, 20-23 October 2013.

[10] W. Yaici, and E. Entchev, "Prediction of the performance of a solar thermal energy system using adaptive neuro-fuzzy inference system", *International Conference on Renewable Energy Research and Applications, ICRERA*, Milwaukee, USA, pp. 601-604, 19-22 October 2014.

[11] E. M. Toygar, A. Yazar, T. Byram, M. Tustan, O. F. Kaya, O. Das, and H. Calmaz, "Design and development of solar flat mirror and heat storage System", *International Conference on Renewable Energy Research and Applications, ICRERA*, Milwaukee, USA, pp. 821-827, 19-22 October 2014.

[12] M. R. Rodríguez-Sánchez, C. Leray, A. Toutant, A. Ferriere, and G. Olalde, "Development of a new method to estimate the incident solar flux on central receivers from deteriorated heliostats", *Renewable Energy*, vol. 130, pp. 182-190, January 2019.

[13] S. Mann, "Compositing multiple pictures of the same scene", *46th Annual IS&T Conference*, Cambridge, Massachusetts, pp. 50-52, 9-14 May 1993.

[14] B. S. Eastwood and E. C. Childs, "Image alignment for multiple camera high dynamic range microscopy", *IEEE Workshop on Applications of Computer Vision*, Breckenridge, USA, pp. 225-232, 9-11 January 2012.

[15] S. Mann and R. W. Picard, "On being 'undigital' with digital cameras: extending dynamic range by combining differently exposed pictures," *48th Annual IS&T Conference*, Washington, USA, pp. 422-428, 1995.

[16] B. Madden, "Extended intensity range imaging", *GRASP Laboratory*, University of Pennsylvania, 1993.

[17] K. Yamada, T. Nakano, and S. Yamamoto, "Effectiveness of video camera dynamic range expansion for lane mark detection", *IEEE Conference on Intelligent Transportation Systems*, Boston, Massachusetts, pp. 584-588, 9-12 November 1997.

[18] K. Yamada, T. Nakano, S. Yamamoto, E. Akutsu, and I. Aoki, "Wide dynamic range vision sensor for vehicles", *IEEE International Conference on Vehicle Navigation and Information Systems*, pp. 405-408, 31 August-2 September 1994.

[19] K. Moriwaki, "Adaptive exposure image input system for obtaining high-quality color information", *Systems and Computers in Japan*, vol. 25, no. 8, pp. 51-60, July 1994.

[20] Z. Chen and G. Mu, "High-dynamic-range image acquisition and display by multi intensity imagery", *Journal of Imaging Science and Technology*, vol. 39, no. 6, pp. 559-563, 1995.

[21] P. Debevec and J. Malik, "Recovering High Dynamic Range Radiance Maps from Photographs", *24th annual conference on Computer graphics and interactive*

techniques - SIGGRAPH '97, Los Angeles, California, pp. 369-378, 3-8 August 1997.

[22] M. A. Robertson, S. Borman, and R. L. Stevenson, "Estimation-theoretic approach to dynamic range enhancement using multiple exposures", *Journal of Electronic Imaging*, vol. 12, no. 2, pp. 219-228, April 2003.

[23] G. C. Holst, *CCD arrays, cameras, and displays*, 2nd ed., Winter Park, FL JCD Publishing, Bellingham, Washington, USA, 1998.

[24] P. Rodrigues and J. P. Barreto, "Single-image estimation of the camera response function in near-lighting", *IEEE Conference on Computer Vision and Pattern Recognition*, Boston, Massachusetts, pp. 1028-1036, 7-12 June 2015.

[25] "JAI AD-081 GE CCD camera user manual", 2013. [Online]. Available: https://www.jai.com/downloads/manual-ad-081ge. [Accessed: 4 May 2018].

[26] S. Mann, "Comparametric equations with practical applications in quantigraphic image processing", *IEEE Transactions on Image Processing*, vol. 9, no. 8, pp. 1389-1406, August 2000.

[27] T. Mitsunaga and S. K. Nayar, "Radiometric self-calibration", *IEEE Computer Society Conference on Computer Vision and Pattern Recognition*, Fort Collins, Colorado, pp. 374-380, June 1999.

[28] S. De Neve, B. Goossens, H. Luong, and W. Philips, "An improved HDR image synthesis algorithm", *16th IEEE International Conference on Image Processing*, Cairo, Egypt, pp. 1545-1548, 2009.

[29] E. Reinhard, W. Heidrich, P. Debevec, S. Pattanaik, G. Ward, and K. Myszkowski, *High dynamic range imaging : acquisition, display, and image-based lighting*, 2nd ed., Elsevier Science, Morgan Kaufmann, Amsterdam, 2010.

[30] Y. Tsin, V. Ramesh, and T. Kanade, "Statistical calibration of CCD imaging process", *8th IEEE International Conference on Computer Vision*, Vancouver, B.C., Canada, pp. 480-487, 7-14 July 2001.

[31] K. Kirk and H. J. Andersen, "Noise characterization of weighting schemes for combination of multiple exposures", *British Machine Vision Conference*, Edinburgh, UK, pp. 1129-1138, 2006.

[32] B. Goossens, H. Luong, J. Aelterman, A. Pižurica, and W. Philips, "Realistic camera noise modeling with application to improved HDR synthesis", *EURASIP Journal on Advances in Signal Processing*, vol. 2012, no. 1, pp. 1-28, December 2012.

[33] M. Mokhtar, I. Rubalcaba, S. Meyers, and M. Chiesa, "Heliostat field efficiency test of beam-down CSP pilot plant: experimental results", *SolarPACES Conference*, Perpignan, France, 21-24 September 2010.

[34] M. Röger, P. Herrmann, M. Ebert, C. Prahl, S. Ulmer, and F. Göhring, "Flux density measurement on large scale receivers", *SolarPACES Conference*, Granada, Spain, 20-23 September 2011.